Polymer 50 (2009) 2786–2792

Contents lists available at ScienceDirect

Polymer

journal homepage: www.elsevier.com/locate/polymer

Multiwalled carbon nanotube cryogels with aligned and non-aligned porous structures

Soon-Min Kwon, Hun-Sik Kim, Hyoung-Joon Jin*

Department of Polymer Science and Engineering, Inha University, Incheon 402-751, Republic of Korea

ARTICLE INFO

Article history:
Received 5 February 2009
Received in revised form
23 April 2009
Accepted 25 April 2009
Available online 3 May 2009

Keywords:
Multiwalled carbon nanotubes
Silk fibroin
Ice-templating

ABSTRACT

Multiwalled carbon nanotube (MWCNT) cryogels were fabricated with aligned and non-aligned porous structures. The MWCNT cryogels contained a major fraction of MWCNTs with a minor fraction of silk fibroin as the structure binder. The morphology of the porous structures was controlled using a sol–gel process of silk fibroin to form the network structures. Microchannel structures were formed by ice-templating. The MWCNT cryogels contained mesopores and formed as monoliths. The MWCNT cryogels with aligned porous structures showed better thermal stability and electrical conductivity than the MWCNT cryogels with non-aligned porous structures due to the advantageous MWCNT interconnections. The morphology of the porous structures was examined by field emission scanning electron microscopy and transmission electron microscopy. The structure–property relationships of the MWCNT cryogels and the performance of the MWCNT cryogels as electrodes were investigated.

1. Introduction

Porous carbon materials, such as carbon aerogels, have many interesting properties, such as high surface area, high electrical conductivity, interconnected porous network structure and extremely low densities. These materials have potential applications in a variety of areas, including catalysts [1], adsorbents [2], electrodes [3] and template materials [4]. Carbon aerogels can be synthesized using a sol–gel process to form gel structures. This process can be monitored by special drying and carbonization processes in an inert atmosphere [5]. Freeze-drying methods are a special drying method that maintains the gel structures, and aerogels prepared using freeze-drying methods are generally known as cryogels. This method is economical, practical and useful. Recently, Yodh et al. synthesized carbon nanotube (CNT) aerogels [6]. CNT aerogels were reported to support at least 8000 times their weight [6] and exhibited good electrical conductivity, 10^{-2} S/cm [7]. In addition, del Monte et al. produced a macroporous 3D architecture of self-assembled CNT using ice-templating [8].

The morphology of the porous materials is an important factor because the nanostructures, pore properties and microstructure have a significant effect on their applications [9,10]. Coasne et al. synthesized ordered and disordered porous carbon by freezing argon, and reported differences between ordered and disordered porous carbon [9]. The most suitable structure morphology of a porous material must be selected for optimal applications. A porous structure can control the formation of aligned/ordered structures or non-aligned/disordered structures. Aligned/ordered porous structures can be synthesized using an ice-segregation-induced self-assembly (ISISA) method using ice-templating or unidirectional freezing techniques [7,8,10,11]. In this method, ice is used as the template. Ice templates are not only formed in situ but are also formed in the microchannels and aligned/ordered porous structures. In addition, they can be easily removed, and are inexpensive and environmentally friendly. On the other hand, non-aligned/disordered porous structures can be synthesized using sol–gel methods, which is termed gelation [12,13]. This forms interconnected solid structures to three-dimensional (3D) network porous structures.

In this study, aligned or non-aligned multiwalled carbon nanotube (MWCNT) cryogels with silk fibroin were fabricated as either a structure binder or solid structure. MWCNT cryogels can be used as biomaterial scaffolds [11,14,15]. Oxidized MWCNTs are quite soluble in water. Therefore, they can be dispersed in an aqueous silk fibroin solution [16]. For this reason, a stable MWCNT-dispersed silk fibroin solution was prepared as a precursor to create aligned and non-aligned porous structures. Aligned MWCNT cryogels were prepared by ice-templating with silk fibroin as the structure binder. Non-aligned MWCNT cryogels were prepared using a gelation method by employing the sol–gel reaction of silk fibroin. This study also examined the morphological, textural and electrical properties of the fabricated aligned or non-aligned MWCNT cryogels.

* Corresponding author. Tel.: +82 32 860 7483; fax: +82 32 865 5178.
E-mail address: hjjin@inha.ac.kr (H.-J. Jin).

0032-3861/$ – see front matter © 2009 Elsevier Ltd. All rights reserved.
doi:10.1016/j.polymer.2009.04.056

2. Experimental

2.1. Preparation of stable MWCNT dispersed in a silk fibroin aqueous solution

MWCNTs (purity of 95%; supplied by Iljin Nanotech, Korea) were produced by thermal chemical vapor deposition (CVD). The as-received MWCNTs were treated with acid to remove the impurities, such as metallic catalysts, using a procedure reported elsewhere [17]. The MWCNTs were treated with an acid mixture (sulfuric acid/nitric acid = 3:1 (v/v)) at 60 °C for 6 h. As a result, carboxylic functional groups were introduced to the surface of the MWCNTs [18]. Cocoons of *Bombyx mori* silkworm silk were supplied by the Boeun Sericulture Farm in Korea. Pure silk fibroin was obtained by boiling the cocoons for 30 min in an aqueous solution of 0.02 M sodium carbonate (Na_2CO_3, 99.5%+, Aldrich), and rinsing them thoroughly with deionized water to extract the glue-like sericin proteins. The extracted silk fibroin was dried at room temperature for 72 h, and then dissolved in 9.3 M lithium bromide (LiBr, ≥99%, Aldrich) at 55 °C for 2 h [16]. The solution was dialyzed in deionized water using Slide-A-Lyzer® dialysis cassettes (Pierce, MWCO 3500, USA) for 36 h. After dialysis, the final concentration of the aqueous silk fibroin solution was 7–8 wt%, which was determined by weighing the remaining solid after drying. Appropriate amounts of the acid-treated MWCNTs were then dispersed in water using an ultrasonic generator (Kodo Technical Research Co., Korea) with a nominal frequency of 28 kHz and a power of 600 W for 1 h at 25 °C. The MWCNT dispersed in water was added at the appropriate amounts to the silk fibroin aqueous solution. Stable MWCNT (0, 3, 6, and 9 wt%) dispersions in an aqueous silk fibroin (2 wt%) solution were prepared [16].

2.2. Fabrication of non-aligned or aligned MWCNT cryogels

The MWCNTs dispersed in the aqueous silk fibroin solution was poured into cylinder-shaped glass molds (diameter 12 mm). Non-aligned MWCNT cryogels (GEL-series) were fabricated using a gelation method, as shown in Fig. 1a. To prepare GEL-3, 15 ml of stable MWCNT (3 wt%) dispersions in an aqueous silk fibroin (2 wt%) solution were left to stand for a few days at 60 °C at pH ~7 to allow setting in the form of an elastic hydrogel through silk fibroin gelation [19]. The prepared MWCNT-dispersed silk fibroin elastic hydrogel was flash-frozen in liquid nitrogen (−196 °C) for a few seconds to freeze the pore liquid, and immediately freeze-dried in a lyophilizer (LP3, Jouan, France) at −50 °C and 0.045 mbar for 48 h. Aligned MWCNT cryogels (ICE-series) were fabricated using ice-templating according to the procedure described elsewhere, as shown in Fig. 1b [11]. The silk fibroin solution with dispersed MWCNTs (2 wt%) was collected in glass molds, which were dipped into a cold bath at a constant rate of 10 cm/h and a constant temperature (−196 °C). The unidirectionally frozen MWCNTs dispersed in the silk fibroins were then freeze-dried in a lyophilizer under steady conditions used in the gelation process. When the freeze-drying process was complete, the aligned or non-aligned MWCNT cryogels were obtained in monolithic form with both the size and shape of the glass molds maintained, as shown in Fig. 1. The aligned and non-aligned MWCNT cryogels prepared with different concentrations of MWCNTs are denoted as ICE-*x* and GEL-*x*, respectively, where *x* indicates the dispersed MWCNT concentration. As control experiments, silk fibroin cryogels were prepared using either ice-templating or gelation methods, as described above, but without the MWCNTs.

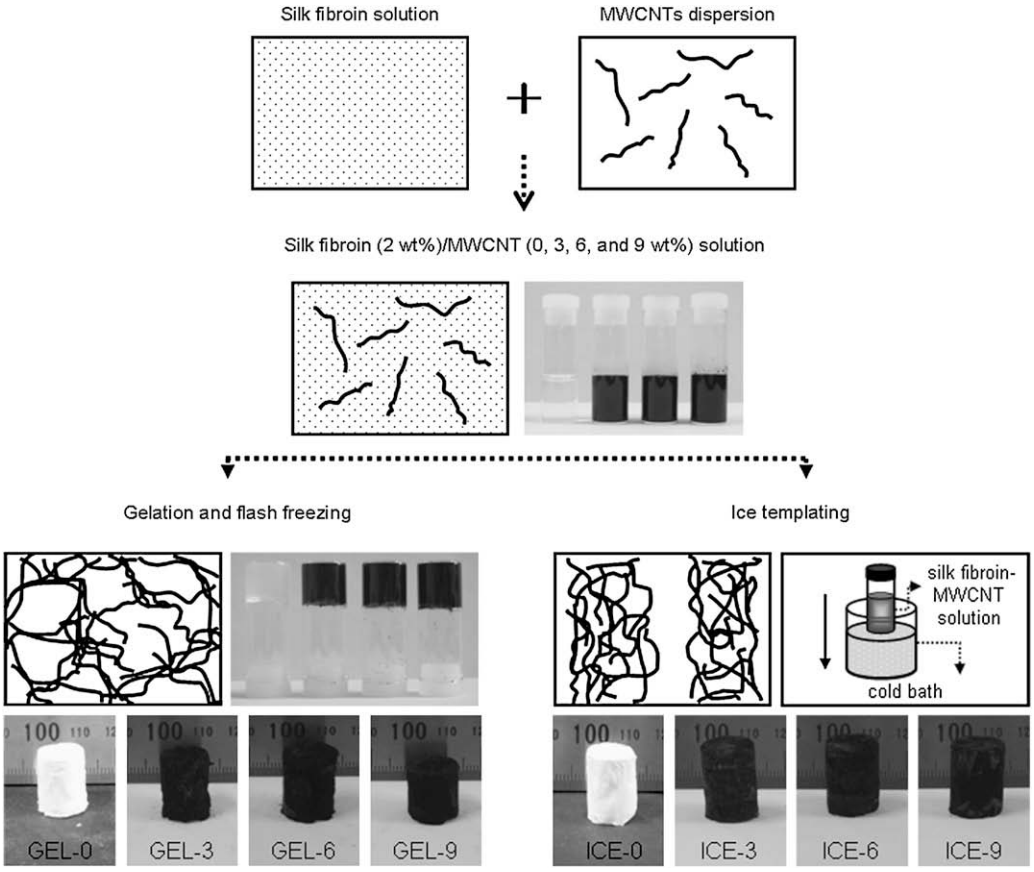

Fig. 1. Schematic diagram of the formation of porous structure with (a) the gelation and flash freezing and (b) ice-templating.

2.3. Characterization

The morphology of the porous structures was observed by field emission scanning electron microscopy (FESEM, S-4300SE, Hitachi, Japan) at an accelerating voltage of 15 kV after coating the samples with a homogeneous Pt layer by ion sputtering (E-1030, Hitachi, Japan). The presence of MWCNTs in the pore structure was confirmed by examining the internal structure of the samples by transmission electron microscopy (TEM, CM200, Philips, Netherlands) at an accelerating voltage of 100 kV. The samples were ground thoroughly into powder. The appropriate amount of sample powder was then dispersed in acetone under ultrasound, and one drop was placed onto a copper grid for TEM observations. The porous properties of the aligned and non-aligned MWCNT cryogels were analyzed from the nitrogen adsorption–desorption isotherms obtained using a surface area and porosimetry analyzer (ASAP 2020, Micromeritics, USA) at −196 °C. The BET surface areas (S_{BET}) were calculated using the Brunauer–Emmett–Teller (BET) theory. The micropore surface area (S_{mic}) and micropore volume (V_{mic}) were obtained using *t*-plot theory. The mesopore surface area (S_{meso}), mesopore volume (V_{mes}) and mesopore diameter (D_{mes}) were calculated in accordance with the Barrett–Johner–Halendar (BJH) theory. Windows-based application software was employed for analysis. Thermogravimetric analysis (TGA, TA instruments, Q50, UK) was used to measure the thermal stability of the aligned and non-aligned MWCNT cryogels. TGA was carried out at a heating rate of 10 °C/min from room temperature to 400 °C under a dynamic nitrogen flow of 10 cm^3/min. The electrical conductivity of the aligned and non-aligned MWCNT cryogels was measured using a four-probe method with an electrical conductivity meter (Hiresta-UP MCP-HT450, Mitsubishi Chemical, Japan). Finally, the electrochemical behavior of the MWCNT cryogels in a cylinder-shaped molder was investigated. A Pt plate (99.99%) was used as the counter electrode and silver–silver chloride (Ag/AgCl) saturated KCl was used as the reference electrode. Cyclic voltammograms (CVs) between −1.0 V and 1.0 V were recorded in a 1.0 M H_2SO_4 aqueous solution. A potentiostat/galvanostat (EG&G 273A) was used for all linear sweep voltammetry (LSV) experiments, and the data was transferred to an IBM-compatible PC controlled through a GPIB interface.

3. Results and discussion

A high-quality MWCNT dispersion was obtained by introducing functional carboxyl groups to the surfaces of the MWCNTs through acid treatments, which improved their solubility [20]. In addition, silk fibroin can easily transform the morphology from spherical micelles to nanofibrils in an aqueous solution by exterior stimulation, such as a decrease in the pH or an increase in temperature [21,22]. Acid-treated MWCNTs can become well dispersed in an aqueous silk fibroin solution. Aqueous MWCNT-dispersed silk fibroin solutions can be used to fabricate silk/MWCNT composites in a straightforward manner. Naturally, silk fibroin forms 3D network structures through a transition of the secondary silk fibroin structures [21]. Fig. 1 shows a schematic diagram of the formation processes of both aligned and non-aligned porous structures in MWCNT cryogels. Fig. 1 also shows images of the MWCNT cryogels fabricated by both gelation and ice-templating. All MWCNT cryogels had a monolithic form, as shown in black, as well as excellent stability. Generally, cryogels are obtained in powder form because the solid network can be destroyed by crystallization of the liquid in the pores during the freeze-drying process [23]. In this case, the MWCNT cryogels exhibit sufficient strength due to the good mechanical properties of silk fibroin.

Fig. 2 shows FESEM images of the GEL-series MWCNT cryogels. Silk fibroin solutions at concentrations ≤5 wt% have been previously studied with respect to hydrogel formation [24–26]. The sol–gel transition depended on the concentration of the protein, temperature, shear and pH. Random coil to β-sheet structural transitions were observed during the hydrogelation process [24–26]. All the GEL-series MWCNT cryogels showed three-dimensional

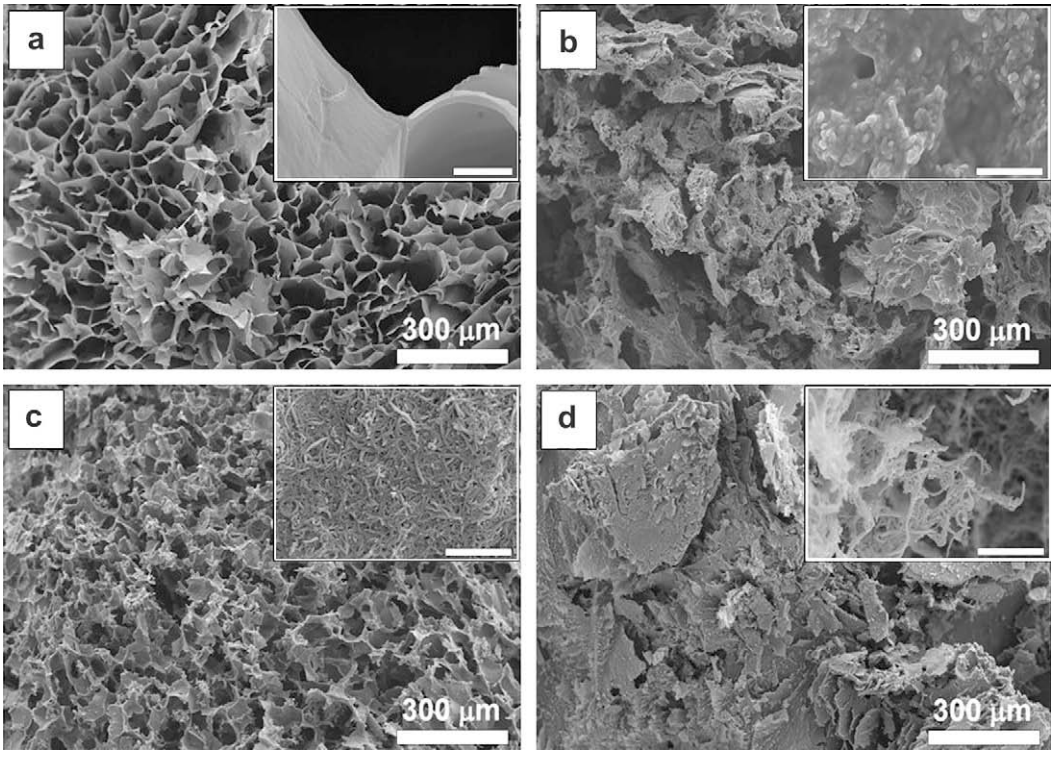

Fig. 2. FESEM images of the porous structure prepared by gelation and flash freezing: (a) GEL-0, (b) GEL-3, (c) GEL-6, and (d) GEL-9. Scale bars (insets): (a) 6 μm and (b–d) 1 μm.

networks and randomly supermacroporous structures. These features generally appear in cryogels fabricated by freeze-drying. As the MWCNT concentration was increased from 3 to 9 wt%, the solid structures became thicker, as shown in Fig. 2b–d. Silk fibroin formed solid structures through the gelation process. The MWCNTs aggregated into solid structures as a result of the sol–gel reaction of silk fibroin. The inset images in the figures show larger magnification images of the surface structures, which indicates that the MWCNTs had been embedded in the GEL-series MWCNT cryogels. Fig. 3 shows FESEM images of the ICE-series MWCNT cryogels. All ICE-series MWCNT cryogels had microchannels and aligned porous structures. As the MWCNT concentration was increased from 3 to 9 wt%, the microchannel solid structures became well aligned and formed more complete polygonal rod shapes than those at low MWCNT concentration, as shown in Fig. 3b–d. In particular, ICE-9 showed well-aligned microchannel structures in the freezing direction with a well-patterned between-channel morphology, as shown in Fig. 3d. In ice-templating, straight and long supermacropores can form through the ice template. In addition, the microchannel structures of the ICE-series MWCNT cryogels were characterized by walls consisting of silk fibroin and MWCNTs enclosing vacant areas where the ice templates were located initially [8]. In this study, when the MWCNT concentration was at least 8 wt%, the walls of the microchannel structures formed in polygonal rod shapes. The inset images in the figures show larger magnification images of the surface structures. This suggests that the MWCNTs constitute the walls of the microchannel structures in the ICE-series MWCNT cryogels. As shown in inset image in Fig. 3a, it is possible to show spherical micelles of silk fibroin, which indicates that the silk fibroin did not gel [21].

The inner morphology of the MWCNT cryogels was observed by TEM to confirm the existence of MWCNTs and determine how they become embedded in the solid structures, as shown in Fig. 4. Fig. 4a shows that the MWCNTs in GEL-9 are embedded in solid structures and covered with silk fibroin. The wide black areas indicate the silk fibroin solid structures. On the other hand, the inner morphology pertaining to ICE-9 shows that the MWCNTs and the silk fibroin were well constructed, and that the MWCNTs were well dispersed in a wall of solid structures, as shown in Fig. 4b. Furthermore, the MWCNTs were interconnected with each other. This suggests that the electrical conductivity and thermal conductivity of the ICE-series MWCNT cryogels are more efficient than those of the GEL-series MWCNT cryogels.

Fig. 5 shows the nitrogen adsorption–desorption isotherms of the MWCNT cryogels. Generally, the nitrogen adsorption–desorption isotherms are used to characterize the specific surface areas and textural properties of the samples. As shown in Fig. 5a, the isotherms of the GEL-series MWCNT cryogels correspond to the IUPAC type IV curves and exhibit a small type H2 hysteresis loop (asymmetrical with adsorption/desorption branches). This suggests that the GEL-series MWCNT cryogels are mesoporous materials with connected pores or poorly defined pores. This is a viable structure for non-aligned MWCNT cryogels [27–29]. The isotherms of the ICE-series MWCNT cryogels correspond to the IUPAC type IV curves and exhibit a small type H1 hysteresis loop (symmetrical with the adsorption/desorption branches), as shown in Fig. 5b. This suggests that ICE-series MWCNT cryogels are mesoporous materials with unconnected pores or a narrow distribution of pore sizes due to the uniform pores in a fairly regular array [28,29]. These results confirm the FESEM findings. Compared with ICE-0, ICE-3 and the GEL-series MWCNT cryogels, there was a significantly higher amount of nitrogen adsorbed on ICE-6 and ICE-9 at an approximate P/P_0 value of ~ 0. This suggests the development of micropore areas. In addition, the hysteresis loops of the GEL-series MWCNT cryogels shifted at a P/P_0 value of 0.75–0.85. This suggests that larger meso- and macropores had developed in the GEL-series MWCNT cryogels than in the ICE-series MWCNT cryogels. Therefore, the GEL-series MWCNT cryogels had a smaller surface area,

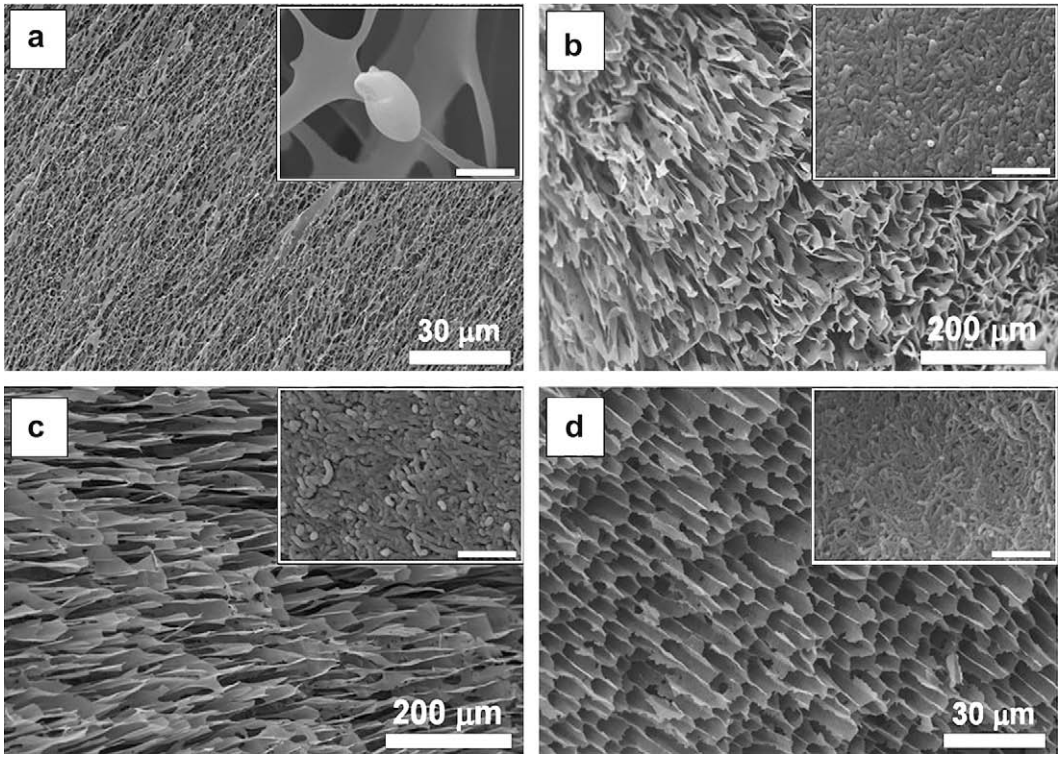

Fig. 3. FESEM images of the porous structure prepared by ice-templating: (a) ICE-0, (b) ICE-3, (c) ICE-6, and (d) ICE-9. Scale bars (insets): (a–d) 500 nm.

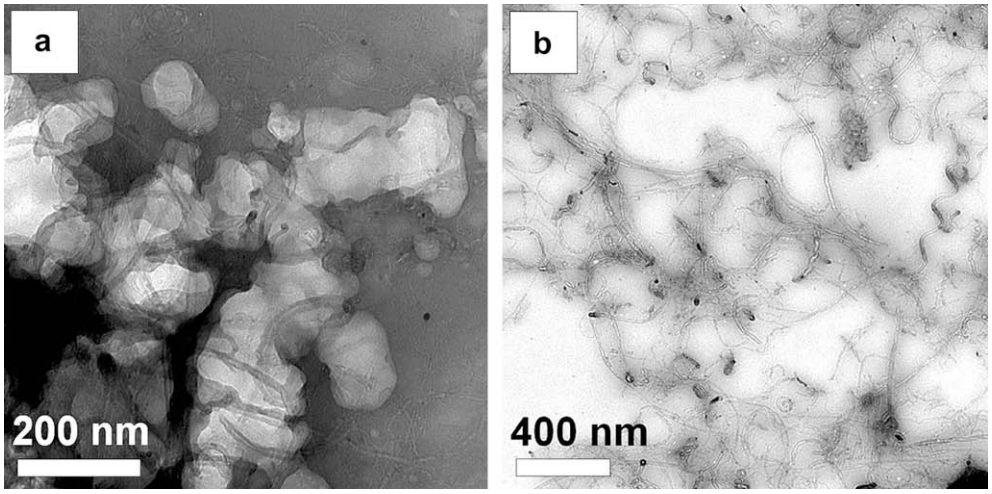

Fig. 4. TEM images of the porous structure: (a) GEL-9 and (b) ICE-9.

than the ICE-series MWCNT cryogels due to the smaller microporosity and relatively larger pore sizes.

Table 1 summarizes the porous properties of the prepared MWCNT cryogel samples with a pore size between 1.7 and 300 nm. The surface areas of the MWCNT cryogels increased with increasing MWCNT concentration. This was attributed to the development of micro- or mesoporosity. A comparison of the GEL-series MWCNT cryogels in terms of mesoporosity revealed only that the ICE-series MWCNT cryogels have a higher number of micro- and mesopores. Moreover, the mesopore size of the ICE-series MWCNT cryogels was relatively constant, whereas that of the GEL-series MWCNT cryogels increased gradually from 15.7 to 25.4 nm with increasing MWCNT content. These results were confirmed by the pore size distributions of the MWCNT cryogels, as shown in Fig. 6. The figure shows that the GEL-series MWCNT cryogels have a main mesopore peak, which shifts to a larger pore size. On the other hand, the main mesopore peak of the ICE-series MWCNT cryogels does not shift and remains relatively constant. This suggests that the network pore structures of the GEL-series MWCNT cryogels were thicker due to the aggregation of MWCNTs caused by the increased MWCNT concentration. In addition, as shown in Fig. 6a, the pore volume corresponding to the main mesopore peak increased, indicating that mesoporosity developed due to the increase in MWCNT concentration. However, microchannel pore structures of the ICE-series MWCNT cryogels were formed using an ice template that grew during the process. Hence, the mesopore diameter of the ICE-series MWCNT cryogels reproduces the size of the ice template. Moreover, the mesoporosity was limited to a constant MWCNT concentration, as shown in Fig. 6b.

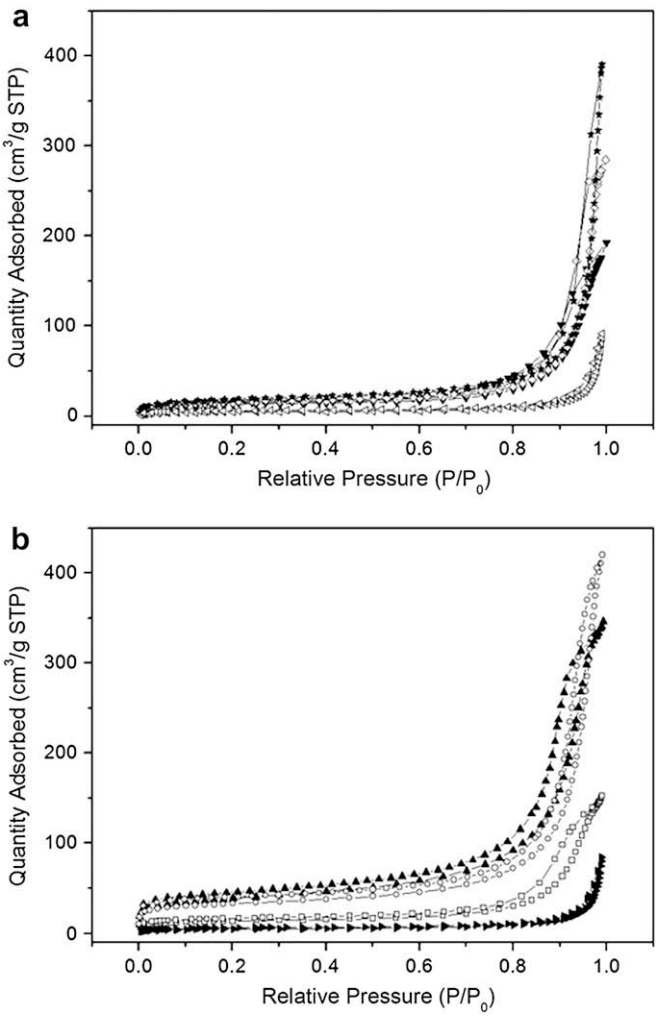

Fig. 5. Nitrogen adsorption–desorption isotherms of (a) GEL-0 (-◁-), GEL-3 (-▼-), GEL-6 (-◇-), and GEL-9 (-★-); (b) ICE-0 (-►-), ICE-3 (-□-), ICE-6 (-▲-), and ICE-9 (-○-).

The thermal behavior of the MWCNT cryogels was examined by TGA. Fig. 7 shows the TGA curves of the MWCNT cryogels obtained in an inert atmosphere. Generally, the mass loss of silk fibroin was characterized by three divided regions. Water evaporates from 35–40 °C to 117 °C, whereas the mass loss at the other low temperatures due to volatile species was quite low, up to 250 °C. On the other hand, silk fibroin degraded and a steep mass loss was observed at above

Table 1
Pore structural parameters of the samples.

Samples	S_{BET} (m^2/g)	S_{mic} (m^2/g)	S_{meso} (m^2/g)	D_{meso} (nm)	V_{mic} (cm^3/g)	V_{meso} (cm^3/g)
GEL-0	20.8	6.3	14.5	32.0	0.0024	0.1364
GEL-3	50.7	18.1	32.6	15.7	0.0079	0.2749
GEL-6	84.1	36.2	47.9	22.1	0.0153	0.6280
GEL-9	115.7	25.7	90.0	25.4	0.0098	0.8609
ICE-0	20.1	6.1	14.0	31.3	0.0028	0.1251
ICE-3	49.9	22.2	27.7	16.6	0.0087	0.2108
ICE-6	138.2	44.9	93.3	15.1	0.0189	0.5088
ICE-9	180.9	61.7	119.2	17.2	0.0251	0.6196

S_{BET}: BET surface area; S_{mic}: *t*-plot micropore area; S_{meso}: *t*-plot external surface area; D_{meso}: BJH desorption average pore diameter; V_{mic}: *t*-plot micropore volume; V_{meso}: BJH desorption cumulative volume of pores between 1.7 and 300 nm in diameter.

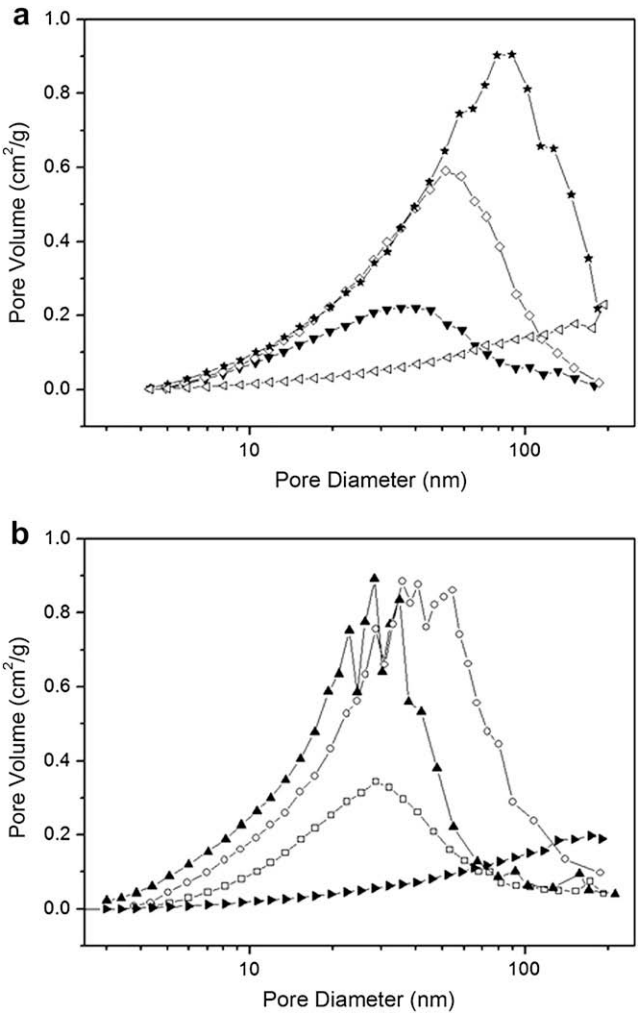

Fig. 6. Pore size distributions (BJH) of (a) GEL-0 (-◁-), GEL-3 (-▼-), GEL-6 (-◇-), and GEL-9 (-★-); (b) ICE-0 (-►-), ICE-3 (-□-), ICE-6 (-▲-), and ICE-9 (-○-).

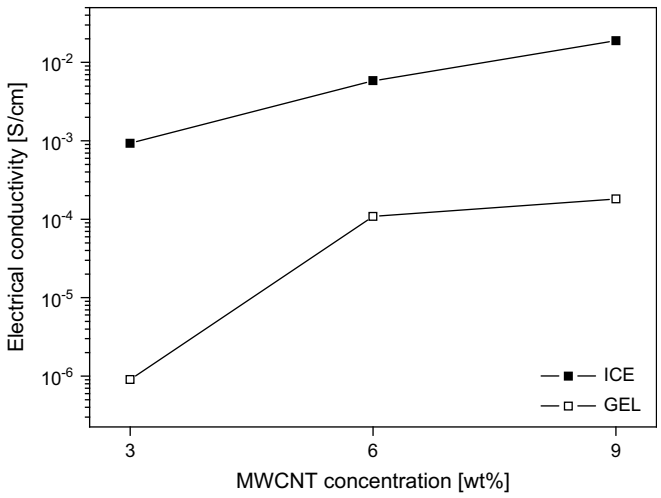

Fig. 8. Electrical conductivity of porous structure prepared by flash freezing and ice-templating.

270 °C [30]. As shown in Fig. 7, the decomposition temperature of silk fibroin in all MWCNT cryogels increased to approximately ~310 °C with increasing MWCNT concentration. This suggests that the thermal stability of the MWCNT cryogels was increased by the incorporation of MWCNTs inside the porous structures. In addition, ICE-9 was not observed in any decomposition region. Therefore, the thermal stability of the MWCNT cryogels is superior to the pure silk fibroin cryogels. Moreover, the thermal stability of the aligned MWCNT cryogels is superior to that of the non-aligned MWCNT cryogels.

Fig. 8 shows the electrical conductivity of the MWCNT cryogels with aligned or non-aligned porous structures. The electrical conductivity of the GEL-series MWCNT cryogels produced from aqueous 3, 6, and 9 wt% MWCNT-dispersed silk fibroin solutions was 9.0×10^{-7} S/cm, 1.1×10^{-4} S/cm and 1.8×10^{-4} S/cm, respectively. On the other hand, the electrical conductivity of the ICE-series MWCNT cryogels produced from aqueous 3, 6, and 9 wt% MWCNT-dispersed silk fibroin solutions was 9.3×10^{-4} S/cm, 5.8×10^{-3} S/cm, and 1.9×10^{-2} S/cm, respectively. Hence, the MWCNT cryogels fabricated using the ice-templating have outstanding electrical properties and thermal stability compared to the MWCNT cryogels fabricated using gelation methods. This suggests that the aligned porous structures benefit from interconnections between the MWCNTs. On the other hand, the MWCNTs are interrupted by the interconnecting pathways of the silk fibroin in non-aligned porous structures. This confirms the findings from the FESEM and TEM images, as shown in Figs. 2–4.

The electrochemical properties of the MWCNT cryogels with aligned and non-aligned porous structures were investigated. Fig. 9 shows the cyclic voltammograms (CVs) at a scan rate of 50 mV/s over a potential range, −1.0 V to 1.0 V. Compared with the GEL-9 electrode (Fig. 9a), the ICE-9 electrode showed an efficient redox reaction over the broader potential range with a higher current

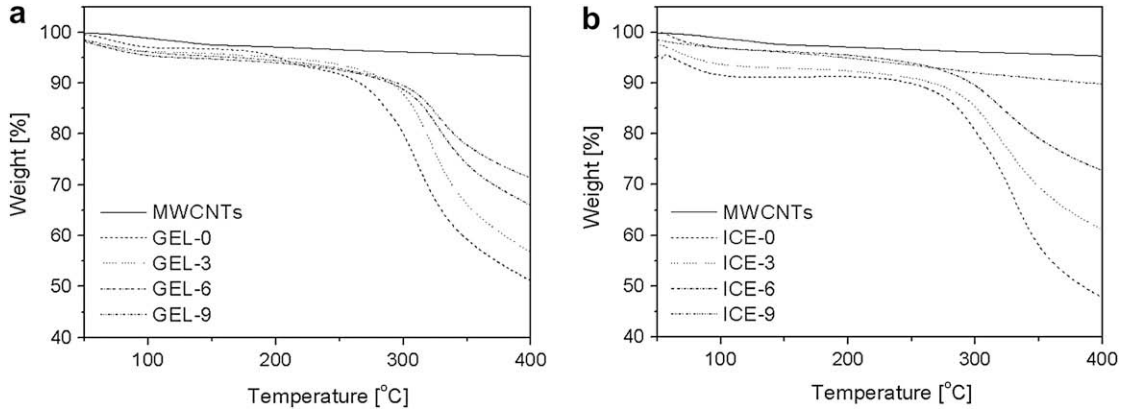

Fig. 7. TGA curves of the porous structure prepared by (a) gelation and flash freezing and (b) ice-templating.

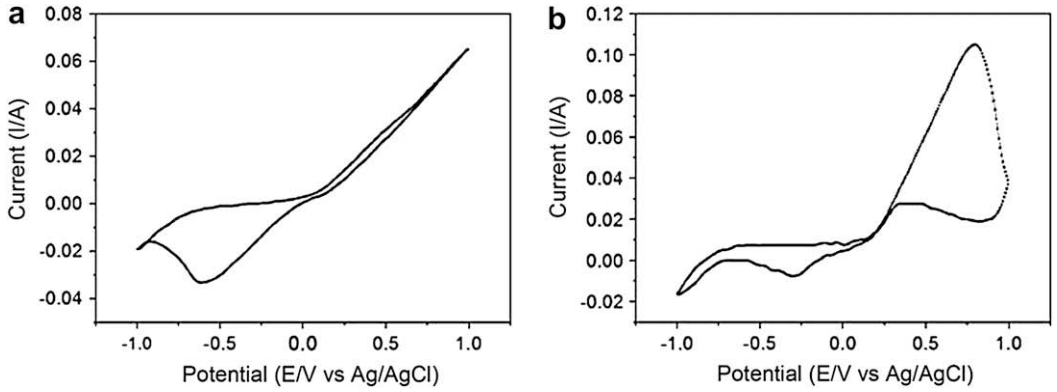

Fig. 9. Cyclic voltammograms of (a) GEL-9 and (b) ICE-9 electrodes in a 1.0 M H_2SO_4 aqueous solution at a scan rate of 50 mV/s.

increases over the potential range than GEL-9, as shown in Fig. 9b. This shows that aligned porous structures and high surface areas improve the accessibility of ions in the electrolyte and provide many active sites for a redox reaction. However, the MWCNT cryogels do not show any viable specific capacitance because the silk fibroin acts as an insulating material. These problems should be addressed in further studies by coating the surface of the MWCNTs with catalyst particles or via the carbonization of silk fibroin. Overall, MWCNT cryogels with aligned porous structures exhibited excellent electrical conductivity, electrochemical properties, and thermal stability. Therefore, aligned MWCNT cryogels can be applied as electrodes in capacitors, as a catalyst in chemical reactions and in biological applications, such as scaffolds for electrically responsive cells including neurons.

4. Conclusions

MWCNT cryogels with aligned and non-aligned porous structures were fabricated using ice-templating and gelation processes, respectively. MWCNT cryogels formed monoliths and showed excellent stability due to the sufficient mechanical strength of the silk fibroin used as a structural binder. The ICE-series MWCNT cryogels contained a porous microchannel structure while the GEL-series MWCNT cryogels possessed a 3D random network structure. The MWCNTs in the GEL-series MWCNT cryogels were embedded and coated with silk fibroin, whereas the MWCNTs in the ICE-series MWCNT cryogels were well dispersed and well interconnected. The ICE-series MWCNT cryogels showed superior thermal stability and good electrical conductivity compared with the GEL-series MWCNTs. In addition, the electrochemical behavior of the aligned porous structure was superior to that of the non-aligned porous structure due to the higher surface area and good accessibility. The ICE-series MWCNT cryogels contained mesopores, approximately 16.3 nm in size, with a micro- and mesoporosity that increased with increasing MWCNT loading. The GEL-series MWCNT cryogels also contained mesopores but the mesopore size increased gradually from 15.7 to 25.4 nm with increasing MWCNT loading due to the aggregation of MWCNTs in the network structures. Control of the porous structures opens up the possibility for novel applications of these MWCNT cryogels in areas associated with biotechnology, catalysis, and electrochemistry.

Acknowledgements

This study was supported by a Korea Science and Engineering Foundation (KOSEF) grant funded by the Korean Government (MOST) (No. R01-2007-000-10438-0).

References

[1] Moreno-Castilla C, Maldonado-Hódar FJ. Carbon 2005;43:455.
[2] Meena AK, Mishra GK, Rai PK, Rajagopal C, Nagar PN. J Hazard Mater 2005;B122:161.
[3] Hwang SW, Hyun SH. J Non-Cryst Solids 2004;347:238.
[4] Tao Y, Kanoh H, Kaneko K. J Phys Chem B 2003;107:10974.
[5] Yamamoto T, Ohmori T, Kim YH. Microporous Mesoporous Mater 2007; 112:211.
[6] Bryning MB, Milkie DE, Islam MF, Hough LA, Kikkawa JM, Yodh AG. Adv Mater 2007;19:661.
[7] Gutiérrez MC, Hortigüela MJ, Amarilla M, Jiménez R, Ferrer ML, del Monte F. J Phys Chem C 2007;111:5557.
[8] Gutiérrez MC, Ferrer ML, del Monte F. Chem Mater 2008;20:634.
[9] Coasne B, Jain SK, Naamar L, Gubins KE. Phys Rev B 2007;76;085416-1.
[10] Nishihara H, Mukai SR, Yamashita D, Tamon H. Chem Mater 2005;17:683.
[11] Abarrategi A, Gutiérrez MC, Moreno-Vicente C, Hortigüela MJ, Ramos V, López-Lacomba JL, et al. Biomaterials 2008;29:94.
[12] Schmidt DF, Hohenesche C, Weiss A, Schädler V. Chem Mater 2008;20:2851.
[13] Chen J, Xue C, Ramasubramaniam R, Liu H. Carbon 2006;44:2142.
[14] Gutiérrez MC, García-Carvajal ZY, Hortigüela MJ, Yuste L, Rojo F, Ferrer ML, et al. J Mater Chem 2007;17:2992.
[15] Hortigüela MJ, Gutiérrez MC, Aranaz I, Jobbágy M, Abarrategi A, Moreno-Vicente C, et al. J Mater Chem 2008;18:5933.
[16] Kim HS, Yoon SH, Kwon SM, Jin HJ. Biomacromolecules 2009;10:82.
[17] Kwon SM, Kim HS, Myung SJ, Jin HJ. J Polym Sci Part B Polym Phys 2008; 46:182.
[18] Kim HS, Park BH, Yoon JS, Jin HJ. Eur Polym J 2007;43:1729.
[19] Vepari C, Kaplan DL. Prog Polym Sci 2007;32:991.
[20] Kim HS, Kang M, Park WI, Kim DY, Jin HJ. Mod Phys Lett B 2008;22:2493.
[21] Chen P, Kim HS, Park CY, Kim HS, Chin IJ, Jin HJ. Macromol Res 2008;16:539.
[22] Kim UJ, Park J, Li C, Jin HJ, Valluzzi R, Kaplan DL. Biomacromolecules 2004; 5:786.
[23] Hüsing N, Schubert U. Angew Chem Int Ed 1998;37:22.
[24] Ayub ZH, Arai M, Hirabayashi K. Biosci Biotechnol Biochem 1993;57:1910–2.
[25] Hanawa T, Watanabe A, Tsuchiya T, Ikoma R, Hidaka M, Sugihara M. Chem Pharm Bull 1995;43:284–8.
[26] Kang GD, Nahm JH, Park JS, Moon JY, Cho CS, Yeo JH. Macromol Rapid Commun 2000;21:788–91.
[27] Tao Y, Noguchi D, Yang CM, Kanoh H, Tanaka H, Yudasaka M, et al. Langmuir 2007;23:9155.
[28] Sing KSW, Everett DH, Haul RAW, Moscou L, Pierotti RA, Rouquérol J, et al. Pure Appl Chem 1985;57:603.
[29] Coasne B, Gubbins KE, Pellenq RJM. Phys Rev B 2005;72. 024304-1.
[30] Motta A, Fambri L, Migliaresi C. Macromol Chem Phys 2002;203:1658.